Chapter 4

Non-invasive Detection and Compression of Fetal Electrocardiogram

Xin Gao

Additional information is available at the end of the chapter

http://dx.doi.org/10.5772/intechopen.69920

Abstract

Noninvasive detection of fetal electrocardiogram (FECG) from abdominal ECG recordings is highly dependent on typical statistical signal processing techniques such as independent component analysis (ICA), adaptive noise filtering, and multichannel blind deconvolution. In contrast to the previous multichannel FECG extraction methods, several recent schemes for single-channel FECG extraction such as the extended Kalman filter (EKF), extended Kalman smoother (EKS), template subtraction (TS), and support vector regression (SVR) for detecting *R* waves on ECG, are evaluated via the quantitative metrics such as sensitivity (SE), positive predictive value (PPV), *F*-score, detection error rate (DER), and range of accuracy. A correlation predictor that combines with multivariable gray model (GM) is also proposed for sequential ECG data compression, which displays better percent root mean-square difference (PRD) than those of Sabah's scheme for fixed and predicted compression ratio (CR). Automatic calculation on fetal heart rate (FHR) on the reconstructed FECG from mixed signals of abdominal ECG recordings is also experimented with sample synthetic ECG data. Sample data on FHR and T/QRS for both physiological case and pathological case are simulated in a 10-min time sequence.

Keywords: noninvasive detection, FECG, FHR, gray prediction, data compression

1. Introduction

Fetal electrocardiogram (FECG) and fetal heart rate (FHR) represent crucial indices for clinical examination and medical diagnosis during pregnancy [1–7, 9–11, 20, 31–36]. In the past decades, multiple systems dynamically monitoring FECG [5, 6, 15, 19, 20, 25–27, 29–31, 35] had been designed for the use of prenatal diagnosis in fetal heart disease, real-time surveillance during both natural and cesarean delivery, as well as the antenatal and intrapartum assessment. Due to the large amount of FECG data for processing in successive monitoring time, enormous storage equipment with durable maintenance is necessary in the design of practical devices [8]: for instance, the double-channel Holter system requires a memory of 82 megabits

for sampled data storage with the resolution of 11 bits and 360 Hz for sampling rate per channel every day. Hence, the design of dynamic system urges solutions for better improvements in practical use for noninvasive FECG detection and compression in portable devices and sensing utilities. A variety of typical FECG extraction techniques [2–5, 9, 14–17, 19, 20, 23–26, 35, 36] had been established for both theoretical study and subsequent practical hardware design [18, 25, 29]. A few classical compression methods [13] introduced for efficient data restoration include polynomial fitting, predictive coding, and orthogonal transform-domain compression, where the principle of data compression is to minimize redundancy at comparatively low penalty of distortion and losing useful information [8]. The correlative models exploiting the correlation information between adjacent QRS waves for sequential prediction suggest an efficient scheme for FECG data compression [8].

The classical schemes for noninvasive FECG extraction over the past 30 years mainly comprise of adaptive signal processing with noise cancellation, spatial filtering techniques, and singular-value decomposition (SVD), to name a few [19, 25]; while the major shortcomings of these schemes were high sensitivity of fetal location and maternal movements, difficulties in extracting P/T waves, and incomplete capture of ECG diagrams [19, 35, 36]. In statistical signal processing, independent component analysis (ICA) [10, 16] aims at computationally separating a mixed signal (with multivariate components) into non-Gaussian signals, where the decomposed signals are assumed to be statistically independent within each other. A variety of methods have been developed for noninvasive FECG extraction since the ICA technique was applied in this research field such as the fourth-order cumulant-based scheme with diagonal approximation proposed by Lathauwer et al. [16], the Joint Approximate Diagonalization of Eigen-matrices (JADE) scheme by Zarzoso [34], Hyvarinen's fast invariant-point method with the ICA principle [10], and the wavelet transform-based infomax algorithm by Jafari and Chambers [12]. Theoretical study on noninvasive FECG extraction methods also employed the ICA-based JADE method with high-order blind identification, the joint detection schemes such as the JADE algorithm with multiple unknown signal extraction, multichannel blind deconvolution [37], and applying the sparse representation of FECG components derived from ICA in the compressed domain [21]. While some previous techniques for noninvasive FECG detection had been considerably mature enough, the challenging issues [4, 28] that have been recognized consist of saving computational cost in abdominal ECG recordings, performing efficient restoration on ECG data, and realizing the practical design (as oriented for low cost, low power, and high integration [29]) for portable FECG monitoring systems. As a result, meeting the balance of recent technical advances with the experimental design on practical systems for noninvasive FECG data-processing devices becomes a crucial task within our investigation.

In this chapter, we present a general study on several categories of algorithms in the field of noninvasive FECG detection, and carry out a performance analysis via several metrics on the state-of-the-art schemes for extracting FECG using sample databases [2, 19, 21]. We proposed a unified approach for the dynamic system design on FECG detection, with a block diagram on noninvasive ECG extraction by collaborating data-processing techniques on weak signal detection

and parameter estimation [8]. Utilizing the correlations between adjacent QRS waves of mixed FECG and maternal ECG (MECG), we derived an improved scheme for ECG compression by predicting minimum mean-square error (MMSE), performing integer wavelet transform, quantization, run-length coding, and arithmetic coding for better realization of FECG data compression [8]. Considerably high compression ratio (CR) with feasible lower distortion in contrast to Sabah's scheme is achieved in condition of preserving the most useful message in the compressed FECG data sequence. Simulations rely on the GM(1, 1) model for gray prediction on CR and percent root mean-square difference (PRD) [8]. We also use the sample synthetic ECG data to fulfill the task of automatic estimation on fetal heart rate (FHR) from the reconstructed FECG.

2. Methodology

The waveform of ECG as depicted in **Figure 1** comprises *P*, *T* waves, and the central QRS interval in a regular period of time [8, 24]. Since continuous ECG monitoring explicitly indicates the exposure of regular heart rate, heartbeat rate with amplitude and duration, prior information on the symptoms of potential heart disease is the most important data reference on medical diagnosis. FECG represents weak signals containing a few strong interferences such as MECG with baseline wander, power line interference and additive noise, while the

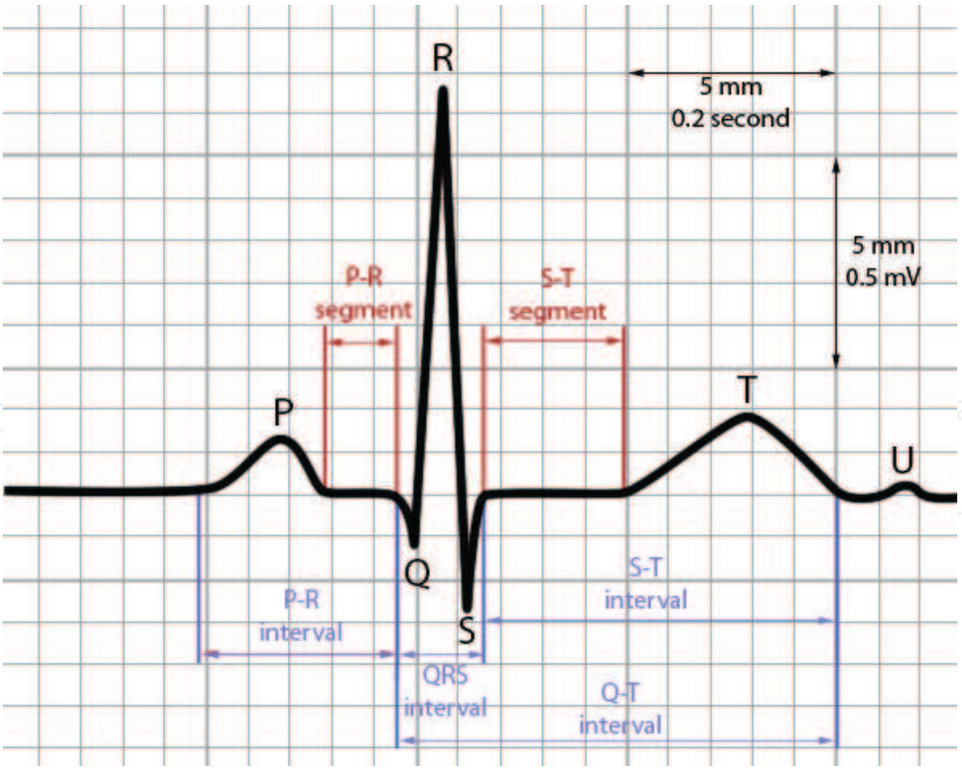

Figure 1. A diagram on the waveform of ECG in a normal period.

noninvasive techniques aim to eliminate these strong disturbances by directly or indirectly measuring FECG via a few properly located electrodes on the maternal abdomen during pregnancy.

Previous schemes such as fetal scalp electrode monitoring, belong to the category of invasive FECG detection (by either scalp electrode or vaginal ultrasound). However, the invasive schemes have obvious shortcomings such as causing pains and injury to the maternal body, and inducing potential risks on uterus infection to the developing fetus. The fetal ECG detection schemes discussed in this chapter belong to noninvasive techniques, indicating no damage or penetration through maternal or fetal skins.

In general cases on noninvasive detection, the mixed ECG was acquired by multiple electrodes in different locations from both thoracic and abdominal regions on a pregnant woman. For instance, the common diagnostic tool for noninvasive ECG recordings usually adopts 8-lead or 12-lead electrode placement (with symmetric electrodes) [2, 20, 41], which had been derived via clinical validation in a couple of periods. The FECG components in multi-lead abdominal recordings are mutually dependent with each other on the fetal position and the electrical conduction toward the maternal abdominal skin. Due to the variations of each component, calculating linear combinations of multichannel outputs generally enhance the signal-to-noise ratio (SNR) of FECG [20]. Meanwhile, since the main electrical axis of the fetal heart position is *a priori* uncertain, in order to increase the possibilities that the calculated nonphysiological leads contain significant FECG components, it is often chosen to compute a set of four linear combinations for equal weights, that is, the position angles correspond with 0°, 45°, 90°, and 135° for the 8-lead placement [2, 20]. Similarly, a 12-lead ECG placement (12 leads calculated using 10 electrodes, in which 6 chest electrodes provide information on the heart's horizontal plane and 4 limb electrodes on the heart's vertical plane) illustrates a more cohesive diagram on the accurate electrical activity of the heart by recording information through 12 different perspectives, where the instruction with specific details on the 12-lead placement guide was illustrated in Ref. [41]. **Figure 2(a)** and **(b)** illustrate the typical 8-lead electrode placement [2, 20] for noninvasive FECG detection and 12-lead electrode replacement [41] for ECG monitoring, respectively.

Among the representative FECG extraction schemes as mentioned above, while blind source separation (BSS) through ICA [16] was previously regarded as having achieved considerably satisfactory results, the demands for multiple signal inputs (typically 8 channels), in addition to the pre-assumption of linearity between MECG and maternal component in the abdominal ECG recordings and monitoring, were put forward as setbacks toward real-time needs in practical implementations [19]. While simulations on the actual relationship between MECG and maternal component in the abdominal ECG were recorded as single-channel inputs, a few other nonlinear schemes proposed recently can be enumerated as given below: the Bayesian filtering framework using the modified dynamic models via several model-based filters such as the extended Kalman filter (EKF), extended Kalman smoother (EKS), unscented Kalman filter (UKF), and wavelet denoising for synthetic ECG data [22, 26]; the ANFIS system [4], in contrast to normalized least mean squares and polynomial networks, for the identification and extraction of FECG from the aligned MECG; the cascaded framework of EKF (for MECG estimation) with ANFIS (for FECG extraction) on both synthetic and actual ECG data in

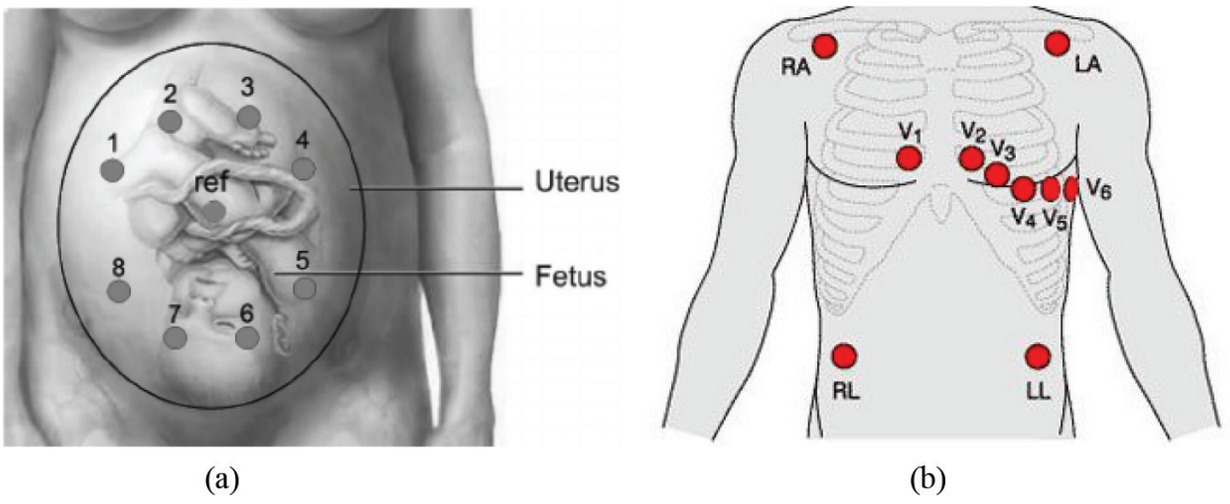

Figure 2. The illustrations of electrodes on: (a) configuration of 8-lead placement for fetal ECG detection; (b) configuration of 12-lead placement for ECG monitoring: the 6 chest electrodes V_1–V_6 show the locations on precordial placements, the 4 limb electrodes show the locations on extremity placements (RA–right arm, LA–left arm, RL–right leg, LL–left leg).

contrast to single EKF, EKS [3], template adaptation (TA) [2], nonparametric detection scheme, and modified template subtraction on sequential data processing [19]; the singular spectrum analysis-based fetal heart signal extraction [9], the fetal heartbeat detection algorithm by the integration of Hilbert transform and nonlinear state-space projections [36], and by supporting vector regression [35]; and a few other clinically adopted noninvasive FECG detection methods from multilead abdominal ECG recordings, see Refs. [4, 5, 15, 17, 20, 33], and the references therein.

For nonstationary signals such as ECG, classical evaluation criteria such as the MMSE principle and predictive coding may generate considerably large prediction errors especially when the amplitude of signal depicts quick fluctuation [8]. Consider two adjacent QRS waveforms with strong relativity in successive phases, let $x(n)$ and $y(n)$ be the input and output of ECG signals, respectively; we observe a sequential data of p points of the former QRS waveform in order to predict the present waveform at the minor cost of generating prediction errors. The predictor output is expressed as [8]:

$$y(n) = \sum_{i=1}^{p} \alpha_i x(n - i - T) \tag{1}$$

where α_i denotes the coefficients of system cascades which can be obtained by Yule-Walker equations and T stands for the average time period between the intervals of R waves.

The prediction error $\varepsilon(n)$ can be calculated via [8]

$$\varepsilon(n) = x(n) - y(n) = x(n) - \sum_{i=1}^{p} \alpha_i x(n - i - T) \tag{2}$$

where a set of consecutive p points represents the orders of correlation predictor.

Since the prediction is processed between two adjacent QRS waveforms, let us denote such kind of prediction as the twin-*R* correlative prediction [8]. In mean-square scales, we express the energy E_p of prediction errors as [8]

$$\begin{aligned} E_p &= E[\varepsilon^2(n)] = E\left\{\left[x(n) - \sum_{i=1}^{p}\alpha_i x(n-i-T)\right]^2\right\} \\ &= E\left\{x^2(n) - 2\sum_{i=1}^{p}\alpha_i x(n)x(n-i-T) + \sum_{i=1}^{p}\alpha_i\sum_{j=1}^{p}\alpha_j x(n-i-T)x(n-j-T)\right\} \\ &= R(0) - 2\sum_{i=1}^{p}\alpha_i R(i+T) + \sum_{i=1}^{p}\alpha_i\sum_{j=1}^{p}\alpha_j R(j-i) \end{aligned} \tag{3}$$

The correlation coefficients of input ECG waves can be calculated via [8]

$$R(m) = \frac{1}{N}\sum_{n=1}^{N-1}x(n)x(n-m) \tag{4}$$

Simplifying Eq. (4) by taking $\frac{\partial E_p}{\partial \alpha_i} = 0$ to obtain a minimum for E_p ($m = 0, 1,\ldots, p-1$) yields [8]

$$\sum_{i=1}^{p-1}\alpha_i R(m-i) = R(m+T), \qquad i = 0, 1, \ldots, p\text{–}1 \tag{5}$$

Constructing the matrix of correlation coefficients by combining Eqs. (3)–(5) yields the linear algebraic equations as follows [8]

$$\begin{bmatrix} R(0) & R(1) & \cdots & R(p-1) \\ R(1) & R(0) & \cdots & R(p-2) \\ \vdots & \vdots & \ddots & \vdots \\ R(p-1) & R(p-2) & \cdots & R(0) \end{bmatrix}\begin{bmatrix} \alpha_0 \\ \alpha_1 \\ \vdots \\ \alpha_{p-1} \end{bmatrix} = \begin{bmatrix} R(T) \\ R(T+1) \\ \vdots \\ R(T+p-1) \end{bmatrix} \tag{6}$$

Solving the equation group in Eq. (6) as above yields the numerical coefficients of each α_i.

The lifting wavelet transform (LWT) has been recognized as a strong implementation when combined with a few algorithms such as integer square zero-tree wavelet coding [8]. Splitting, predicting, and updating symbols, are three steps in the lifting scheme of a typical LWT. The proposed scheme is presented as follows: the first step is to split the ECG data sequence $\{e_j\}$ into two sequences $\{o_{j\text{-}1}\}$ and $\{e_{j\text{-}1}\}$ that stands for odd and even numerals via [8]

$$\text{split } (e_j) = (e_{j-1}, o_{j-1}) \tag{7}$$

Second, with respect to the predictor filter group *P* and the earlier even sequence $\{e_{j\text{-}1}\}$, the odd sequence $\{o_{j\text{-}1}\}$ is predicted by exploiting correlativity information such as [8]

$$o_{j-1} := o_{j-1} - P(e_{j-1}) \tag{8}$$

The last step of updating claims that some integral characteristics as those of integrity for the original $\{e_j\}$ need to be preserved for constructing a better subset $\{e_{j\text{-}1}\}$. As a result, we adopt an updating filter U that exploits the discrepancy between a specific parameter (i.e., mean, variance, or wavelet vanishing moments) and $\{e_j\}$, where this step is proceeded by [8]

$$e_{j-1} := e_{j-1} + U(o_{j-1}) \tag{9}$$

The inverse transform of LWT for signal reconstruction can be similarly expressed via [8]

$$\begin{cases} e_{j-1} := e_{j-1} - U(o_{j-1}) \\ o_{j-1} := o_{j-1} + P(e_{j-1}) \\ e_j = \text{Merge}\,(e_{j-1}, o_{j-1}) \end{cases} \tag{10}$$

The iteration procedures as performed in Ref. [8], applied a (4, 2) LWT for the decomposition and reconstruction of ECG signals, which can be proceeded by [8]

$$\begin{cases} o_j[n] := e_{j-1}[n] + \left\lfloor \frac{1}{16}\left\{(e_{j-1}[n+2]) - 9(e_{j-1}[n+2]) + e_{j-1}[n-1]) + e_{j-1}[n-1]\right\} + \frac{1}{2} \right\rfloor \\ e_j[n] := e_{j-1}[n] + \left\lfloor \frac{1}{4}(o_j[n] + o_j[n-1]) + \frac{1}{2} \right\rfloor \end{cases} \tag{11}$$

where $\lfloor . \rfloor$ denotes the execution of the round-off operation.

The advantages of LWT compared to other wavelet transform methods are displayed in the following scenarios [8]: (i) less dependence for the down-sampling of low pass and high pass signal components and easier realization on the inverse operation of LWT; (ii) reduced execution times by avoiding calculating floating points coming from the integer coefficients; (iii) the implementation of hardware circuits is also much easier; and (iv) guaranteed quality for signal recovery free of boundary continuation in any type.

The procedure of our proposed twin-*R* correlation predictor for improving sequential ECG compression is presented as below [8]: let us denote the implement D as the first-order time delay and P_i as the location of the ith R-wave; $\mathbf{A}_j = \{\alpha_{j,0}, \alpha_{j,1}, \ldots, \alpha_{j,p\text{-}1}\}$ stands for the aggregated coefficients for the twin-R interval of the jth ECG sequence. We take the following steps to perform this task:

Step 1. For the original ECG signal with length N, initially perform the first-order prediction to reduce the DC components of the signals; let $z(n)$ be the redundancy within smooth district of the ECG samples calling for elimination, the residual term $z(n)$ is now expressed as

$$z(n) = x(n) - x(n-1), \qquad n = 0, 1, \ldots, N-1. \tag{12}$$

Step 2. While P_i, the locations of R-wave for each QRS waveform, have been identified, compute each T_i by deducing $T_i = P_{i+1} - P_i$, and estimate the central position of the adjacent twin-R

waves, where $m_i = (P_{i+1} + P_i)/2$. This step speeds up higher recognition rate and operation time, and bears negative effects such as noise interference or baseline shift.

Step 3. Perform the correlation prediction for $z(n)$ similar to Eq. (2):

$$d(n) = z(n) - \sum_{k=0}^{p-1} \alpha_{j,k} z(n - i - T_{i-1}), m_i - l \le m_i + l, l = \min(m_{i-1} - m_{i-2}, m_i - m_{i-1})/2, i = 1, \ldots, N_j. \tag{13}$$

where $d(n)$ denotes the signal of prediction error, p and N_j stand for the order of predictor and the R-wave counts of the jth ECG data sequence, respectively. Without loss of generality, we adopt $p = 4$. The kth prediction coefficient $\alpha_{j,k}$ of each compressed 16-bit ECG sequence was obtained via the splitting process in Step 1. Due to the slow drift for the QRS waveform, an interval of 30 seconds was used to partition this data stream. Note that we implemented the same predictors for continuous QRS waveforms of the same ECG data in order to reduce computational cost and enhance the efficiency for ECG data compression.

Step 4. Update the (4, 2) LWT on the signal $d(n)$ via Eq. (12), where the length of $w(n)$ is preserved as N. For the subband signal $w(n)$ containing $\{o_i(n) = 1,2,3,4\}$ and the approximated signal $e_4(n)$, their length are constructed as $N/2$, $N/4$, $N/8$, $N/16$, and $N/16$, respectively.

Step 5. Perform scalar quantization, run-length coding, and arithmetic coding for $w(n)$. While a few zero-coefficients appear after quantization toward $w(n)$, these successive zeros can be removed via run-length searching so as to shorten the ECG data sequence. Variable quantization coefficients are selected in this procedure; after run-length coding each ECG data sequence is merged by three parts: the constructed bit streams, vector P_i for R-wave localization, and the twin-R predictor coefficients $\mathbf{A}_j = \{\alpha_{j,0}, \alpha_{j,1}, \ldots, \alpha_{j,p-1}\}$.

The flowchart of this scheme as described above is depicted in the block diagram of **Figure 3**, where the prediction step is associated with the compressed ECG data stream.

Since the proposed scheme is invertible for decompression, we need to observe the correlativity and fluctuation tendency between two sequential ECG data; hence, a Lemma is presented for the derivation of ECG data prediction via the single-variable gray model [8].

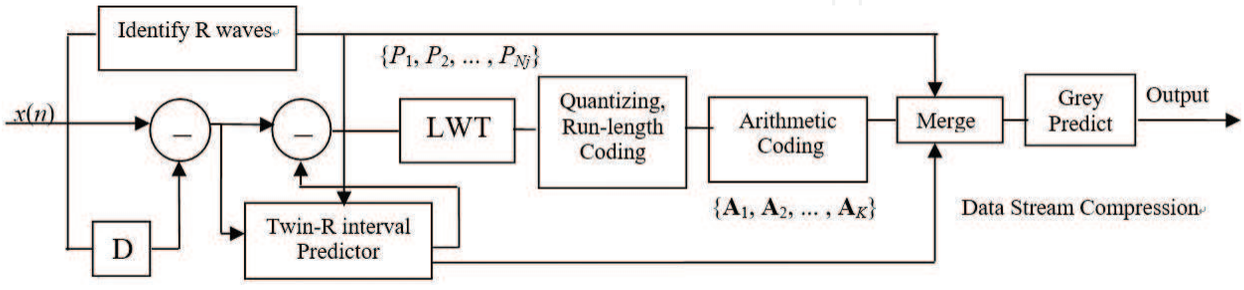

Figure 3. The block diagram of unified twin-R predictive method for ECG sequential data compression.

Lemma 1 [8]: Consider a stationary sequence $T_0 = \{T_0(k) \mid k = 1,\ldots, n\} = \{T_0(1),\ldots, T_0(n)\}$, where k represents the time point. Let us observe a number of m sequences as reference where $T_i = \{T_i(k) \mid k = 1, 2,\ldots, n\} = \{T_i(1), T_i(2),\ldots, T_i(n)\}$, $i = 1, 2,\ldots, n$. Define ξ_k as the correlation coefficient of the kth reference sequence with respect to the starting sequence T_0 at time k,

$$\xi_k = \frac{\min_i \min_k |T_0(k) - T_i(k)| + \rho \max_i \max_k |T_0(k) - T_i(k)|}{|T_0(k) - T_i(k)| + \rho \max_i \max_k |T_0(k) - T_i(k)|} \tag{14}$$

where $\rho \in [0,1)$ denotes the resolution coefficient (and without loss of generality it is often taking expectation of $\rho = 0.5$), $\min_i \min_k |T_0(k) - T_i(k)|$ and $\max_i \max_i |T_i(k) - T_0(k)|$ represents the minimum and maximum difference value between two-levels, respectively. In the gray system theory, $r_i = \frac{1}{n}\sum_{k=1}^{n} \xi_k$ denotes the relevance of sequence T_i to T_0. Geometric similarity on two sequences reflects the degree of correlativity.

Consider the ith sequence $T_i = \{T_i(1), T_i(2),\ldots, T_i(n)\}$, the initialized sequence of original T_i is written as $\overline{T} = (1, T(2)/T(1), \ldots T(n)/T(1))$, and the correlation factor σ_i can be computed via $\sigma_i = \sum_{k=1}^{N} kT_i(k) - \sum_{k=1}^{N} T_i(k) \sum_{k=1}^{N} \frac{k}{n}$, which has the possibility of being either positive or negative. For instance, in the simplest case of $i = 1, 2$, the sequential expression of T_i is formulated as [8]

$$T_i = \left(1, \frac{T_i(1)}{T_i(2)}, \frac{T_i(1)}{T_i(3)}, \ldots, \frac{T_i(1)}{T_i(k)}\right), i = 1, 2; k = N \tag{15}$$

According to Lemma 1, the degree of correlativity is measured by solving Eq. (14). Note that if $\text{sign}(\sigma_1/\sigma_n)\text{sign}(\sigma_2/\sigma_n) = 1$, a positive relevance is justified between T_1 and T_2; conversely, a negative relevance is justified when $\text{sign}(\sigma_1/\sigma_n)\text{sign}(\sigma_2/\sigma_n) = -1$. In more general cases such as ECG data sequence, the correlation factor σ_n can be approximately estimated via [8]

$$\sigma_n = \sum_{k=1}^{n} k^2 - \left(\sum_{k=1}^{n} k^2\right) \Big/ n \tag{16}$$

In the gray system theory, the single variable GM(1, 1) model is often applied to predict the upcoming sequence number and estimate the missed numerical values between time intervals, for the processing of ECG data, we just equalize the corresponding parameters in the time domain, and deduce the gray predictor in the scenario as follows:

The least square (LS) update consists of a whitening procedure through constructing a differential equation in the whitening process with its estimate, and a discretization process for the residuals, which is formulated as [8]:

$$\frac{dT_i^{(1)}}{dt} + aT_i^{(1)} = u, \hat{a} = (a, u)^T \tag{17}$$

$$\hat{\mathbf{a}} = (\mathbf{B}_i^T \mathbf{B}_i)^{-1} \mathbf{B}_i^T \mathbf{Y}_1 \tag{18}$$

$$\mathbf{B}_i = \begin{bmatrix} -\frac{1}{2}(T_i^{(1)}(1) + T_i^{(1)}(2)) & 1 \\ -\frac{1}{2}(T_i^{(1)}(2) + T_i^{(1)}(3)) & 1 \\ \vdots & \vdots \\ -\frac{1}{2}(T_i^{(1)}(n-1) + T_i^{(1)}(n)) & 1 \end{bmatrix}, \mathbf{Y}_i = \begin{bmatrix} T_i^{(1)}(2) \\ T_i^{(1)}(3) \\ \vdots \\ T_i^{(1)}(n) \end{bmatrix} \tag{19}$$

where $\mathbf{B}_i$ and $\mathbf{Y}_i$ denote the data matrix and data vector of GM(1, 1) model, respectively.

A general solution to the matrix equations above is given by [8]

$$T_i^{(1)}(k+1) = \left(T_i^{(0)}(1) - \frac{u}{a}\right)e^{ak} + \frac{u}{a} \tag{20}$$

Determining the model parameters (a, u) yields the past or upcoming numerical values from this predictive GM(1, 1) model. Note that the constructed gray model indicates coincidence with the time-variant extrapolate prediction. In harsh conditions, due to the scarcity of prior information and ambiguity of system on ECG data processing, this predictive GM model is useful since only four adjacent continuous data points are needed from the least data sample.

Because the quality of FECG reflects crucial information on fetal heart rate (FHR) and its beat-to-beat variability [9], the cascaded system design for noninvasive FECG extraction may often involve a post-processing stage such as adaptive noise cancellation or wavelet denoising [12, 22, 34]. FHR is usually estimated via the ratio of 60 to the average time period (s) on a sequence of adjacent intervals from R waves, while estimating FHR technically requires shaping fetal QRS complexes by capturing data via multichannel maternal abdominal ECG recordings [2, 15, 19–21, 23, 26, 30, 32], and by adopting a few other sensing technologies through the Doppler ultrasound devices [37], fetal phonocardiography [1], as well as superconducting magneto-cardiography [33]. Wearable devices on ECG rhythm recording via potential mapping on the wrist/arm surface skin [42] also urge collaborative concerns from industry field toward our theoretically proposed algorithmic study.

3. Performance metrics

The diagnostic tests in biomedical engineering often employ a set of performance metrics in order to evaluate the validity of tests in the subjects on study. In ECG detection, the parameters of true positive (TP), false negative (FN), and false positive (FP) are called from the counts of detected R-peaks. We denote TP as the number of correctly detected R peaks, FN stands for the number of missed R peaks, and FP represents the number of noise spikes detected as R peaks. Hence, the measures of sensitivity (SE) and positive predictive values (PPV) are formulated as [19, 30]:

$$SE = \frac{TP}{TP + FN} \times 100\% \tag{21}$$

$$PPV = \frac{TP}{TP + FP} \times 100\% \tag{22}$$

The *F*-score, known as the harmonic mean of SE and PPV, is expressed as [2, 21]:

$$F\text{–}score = 2 \cdot \frac{SE \times PPV}{SE + PPV} = \frac{2 \times TP}{2 \times TP + FP + FN} \tag{23}$$

Since the total number of *R*-wave peaks is the sum of TP, FN, and FP, the detection error rate (DER) is now denoted as [30]:

$$DER = \frac{FP + FN}{TP + FP + FN} \times 100\% \tag{24}$$

For each DER, the metric of accuracy = 1 – DER yields the same expression as defined in Ref. [19].

The percent root mean-square difference (PRD) represents a fidelity measure for some data compression scheme on the reconstructed/predicted signal in contrast to the original ECG, where the PRD value is numerically calculated as follows [13]:

$$PRD = \frac{\sqrt{\sum_{n=1}^{p} [x(n) - y(n)]^2}}{\sum_{n=1}^{p} x^2(n)} \times 100 \tag{25}$$

where $x(n)$ and $y(n)$ correspondingly represent samples of the original and the reconstructed/predicted ECG data sequences and the length of sequence is p.

Regarding the compression ratio (CR) defined as the proportion of uncompressed size to compressed size for a finite data sequence, or the ratio of uncompressed data rate to compressed data rate for streaming media signals of infinite size such as video or audio [38], for each compression scheme, there is a PRD value corresponding to a required CR.

For synthetic ECG data, consider the abdominal ECG $w(n)$ in case of a single-channel dynamic model, which is nonlinearly synthesized via the MECG $m(n)$, FECG $f(n)$, and the additive white noise $\eta(n)$, and hence, the composite signal is modeled as [19]:

$$w(n) = \hat{m}(n) + \hat{f}(n) = \hat{m}(n) + f(n) + \eta(n) \tag{26}$$

where $\hat{m}(n)$ and $\hat{f}(n)$ denote the nonlinear expressions of MECG and FECG, respectively. Since the noise power in $\eta(n)$ can be adjusted to test the performance of each noninvasive FECG detection scheme [19, 30], for some ECG data sequence with a length of p periodical R peaks, the fetal to maternal signal-to-noise ratio (fmSNR) can be calculated via [19]:

$$fmSNR = 10\log_{10}\left(\frac{\sum_{n=1}^{p}[\hat{f}(n)]^2}{\sum_{n=1}^{p}[\hat{m}(n)]^2}\right) \tag{27}$$

Up till now, we have presented a concise study for the keynote noninvasive techniques and quantitative metrics on FECG detection, with an emphasis on single-channel FECG extraction via nonlinear dynamic models. We proposed a flowchart of processing ECG data sequence by means of LWT and the unified twin-*R* correlation predictor by implementing GM(1,1) model for ECG data compression.

In the next section, we will present three sets of experiments for the qualitative and quantitative evaluation on several noninvasive FECG detection schemes [2, 19, 21], the proposed twin-*R* correlative ECG compression scheme via a widely used ECG database [8], and automatic FHR estimation over a sample sequence of synthetic ECG data [40].

4. Experimental results

We employ sample ECG data from several databases to perform our experimental study: the CinC Challenging Data as referenced in Ref. [2] (also known as the Physionet challenge dataset in Ref. [21]), a noninvasive fetal ECG database in Ref. [19], sample ECG sequences from MIT-BIS Arrhythmia Dataset [8], and some synthetic ECG data from Dr. Igal A. Sebag's example [39]. The main set of experiments with demographic data on sample patients with clinical/synthetic information were summarized in **Table 1**.

The first set of experiments mainly recorded the quantitative evaluations on several representative noninvasive FECG detection schemes based on single-channel abdominal ECG recordings. We studied the test by Panigrahy and Sahu [19] where the QRS complex of FECG displays the most visible features after the preprocessing step of eliminating baseline wander and power line interference from MECG, then each scheme using noninvasive FECG database was implemented to test the detection performance within 60 s of measuring *R* waves.

The numerical results for SE, PPV, *F*-score, and DER on nine methods for FECG detection are illustrated in **Table 2**, where the first column chronologically enumerated the tested FECG detection schemes which correspond to the average score on each measure for the recorded R waves, and the last column specified the range of accuracy over a certain length of time duration [2, 19, 21].

From **Table 2**, we justify that the SE metric on eight FECG detection schemes achieved over 90% except the TA scheme; the metrics of PPV and *F*-score on seven schemes reached over 90% except for SVD and TA; regarding DER, SVD shows the worst performance while it is still as low as 18.7%. Among all the five parameters on the referred quantitative analysis, EKS + ANFIS displays the best overall scores for each metric, while EKF + ANFIS indicates the second best results on *F*-score, DER, and other range of accuracy.

Datasets	Techniques	Demographic data	Comments
Set 1: CinC Challenging [2]; and Set 2: Noninvasive FECG databases [19]	Nine schemes on noninvasive FECG detection	Set 1: 10 pregnant women, ages ranging from 21 to 33 years (27.1 ± 4.3 years), gestational age: 20–28 weeks (25.0 ± 2.5 weeks). Set 2: Uncertain number of patients, gestational age: 21–40 weeks	Set 1: Comprises of 24 clinically acquired abdominal recordings (20-min each), healthy and pathological patients were both present while no ectopic beats detected for either mother or fetus. Set 2: Includes 55 multichannel ECG recordings
Set 3: MIT-BIS Arrhythmia database	Both linear and twin-*R* correlative predictors; (4, 2) LWT compression; GM(1, 1) grey prediction	Set 3: Sequential ECG data on 25 men aged 32–89 years and 22 women aged 23–89 years were included in the subjects, in which approximately 60% were inpatients.	Set 3: Contains a sum of 48 half-hour excerpts of two-channel, 24-hour ECG recordings selected from 47 subjects (there are two records from the same subject) studied by the BIH Arrhythmia Laboratory at MIT in 1975–1979.
Set 4 and Set 5: both samples on synthetic maternal and fetal ECG data;	Adaptive least-mean-square (LMS) or recursive-least-square (RLS) noise cancellation; dynamic thresholding	Set 4: Provides no specific details on the average gestational age, typically in the third trimester (28–40 weeks), normal pregnancy; Set 5: Gestational age of fetus are ∼40 weeks (right before delivery), including samples of physiological and pathological fetus.	Set 4: Synthetic data simulating maternal heart rate of 80–90 bpm with peak voltage 3.5 millivolts and fetal heart rate distributed from 120 to 160 bpm with peak voltage ∼0.2 millivolts. Set 5: similar synthetic data with maternal heart rate of 65–85 bpm and fetal heart rate of 110–150 bpm and T/QRS range of 0.05–0.1 [43].

Table 1. Summary on the main set of experiments for noninvasive techniques on ECG detection and monitoring.

Detection scheme	SE (%)	PPV (%)	*F*-score (%)	DER (%)	Range of accuracy (%)
SVD	90.2	89.2	89.7	18.7	70.6–88.3
EKF	91.5	93.3	92.4	14.2	78.1–97.5
TS	92.0	90.9	91.5	15.7	71.3–91.9
Nonparametric	93.2	92.1	92.7	13.7	79.1–92.3
EKS	92.6	93.6	93.1	13.0	79.1–92.5
TA	86.3	85.5	85.9	16.9	74.8–93.1
EKF + ANFIS	92.8	94.9	93.8	11.8	81.1–94.2
EKS + ANFIS	93.8	96.0	94.9	9.80	83.8–97.6
CS-based ICA	92.5	92.0	92.2	16.5	80.2–96.4

Table 2. Quantitative scores of average SE, PPV, F-score, DER, and range of accuracy on noninvasive FECG detection schemes using a sample FECG database (duration = 60 s).

The second set of experiments was conducted by using the standard database on MIT-BIS Arrhythmia [8] with some original sample data of mixed MECG and FECG. We first investigate the predicted output of errors in comparison to real data from a mixed ECG sequence. **Figure 4** displays four subplots, where (a) depicts an original sequence in time interval [0:1600]

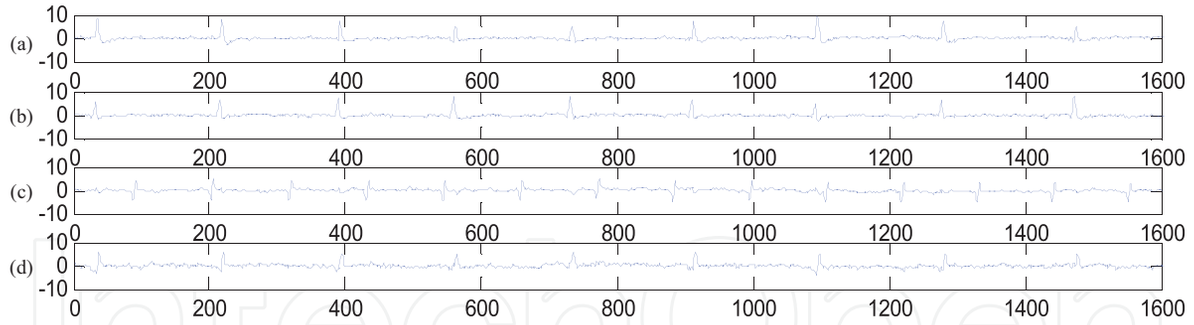

Figure 4. (a) Originally detected FECG; sequential data output by: (b) single linear prediction; (c) fourth-order linear prediction; (d) twin-*R* correlative prediction. Peak voltage denotes the location of *R* waves.

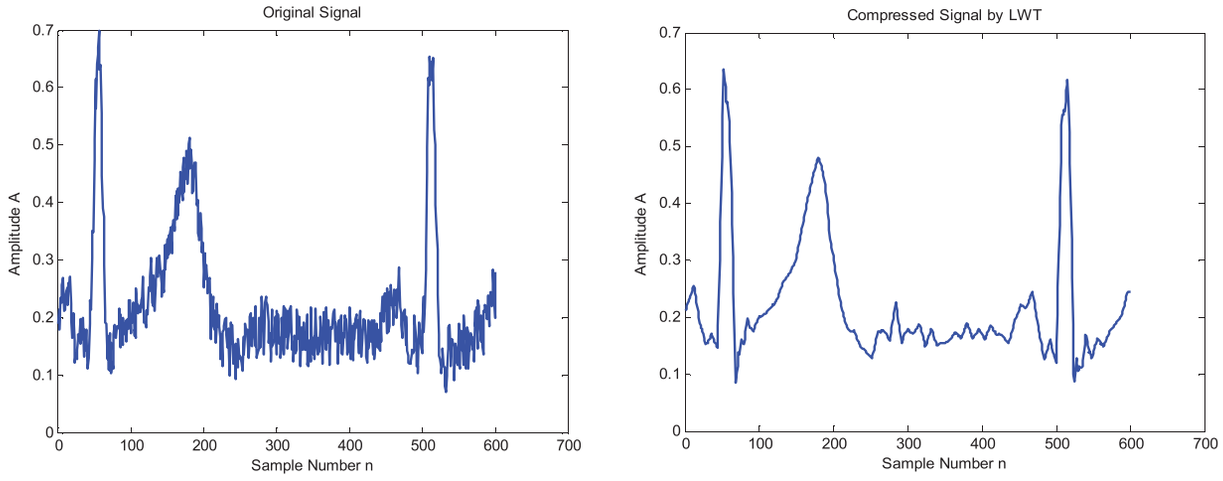

Figure 5. Proposed scheme: (a) original samples (SNR = 10 dB); (b) compressed output via (4, 2) LWT.

of the extracted FECG, (b) illustrates the first-order linear prediction, (c) presents the fourth-order linear prediction, and (d) shows the output of twin-*R* correlative prediction. We justify that the fourth-order predictor contains more false detections but less average errors comparing to the first-order predictor, while the proposed twin-*R* correlation predictor shows reduced average errors in contrast to the former two linear predictors [8].

We applied LWT for sequential ECG compression in time interval [400:1000] with additive random white noise (fmSNR = −10 dB). **Figure 5** displays the original ECG and its compressed output. Comparing **Figure 5(b)** to **Figure 5(a)**, we justify that the compressed ECG preserved most details of the original data with mild penalty of energy lost in the amplitude which comes from the quantization error as well as the loss from round-off decomposition in LWT.

Let us employ the compression ratio (CR) and percent root mean-square difference (PRD) [8, 12] to measure the quantitative compression performance on sequential ECE data: the tests as described below randomly selected 24 cases out of 48 from MIT-BIS Arrhythmia Database as testing samples. The proposed scheme recorded PRDs in a range of variable CRs with different quantization coefficients in comparison to those obtained by the Sabah's method.

	CR	2.0	3.0	5.0	7.0	9.0
PRD	Sabah	2.10	3.22	4.71	6.09	7.68
	Proposed	1.49	1.81	2.75	3.78	5.01
	CR	11.0	13.0	15.0	17.0	19.0
PRD	Sabah	9.33	11.1	12.3	14.0	16.8
	Proposed	6.32	7.67	9.20	11.3	13.6

Table 3. PRD comparison: the proposed scheme versus Sabah's.

We averaged each numerical value of PRD that corresponds to different CR, and enumerated the numbers on both the two schemes in **Table 3**. From the column comparison, we justify that by gaining the same CR ranging from 2.0 to 19.0, our scheme achieved much smaller PRDs than those of Sabah's, which suggests availability of achieving lower distortion rate by the proposed correlative prediction.

While the CR is under determination for both schemes on compression, let us consider CR as time points and PRD as the sequential output, a GM(1, 1) for the "time-sequence" T_1, T_2 is now constructed in order to obtain the predictive value of PRDs. From Eqs. (14) to (16), we are able to justify the positive correlativity between T_1 and T_2. From Eqs. (17) to (20), the solution to predictive GM(1, 1) model after LS updates and iterations is formulated as [8]:

$$T_1: \quad {T_1}^{(1)}(k+1) = (2.10 - 328.91)e^{-0.0026784k} + 328.91 \tag{28}$$

$$T_2: \quad {T_2}^{(1)}(k+1) = (1.49 - 150.95)e^{-0.0049531k} + 150.95 \tag{29}$$

Table 4 illustrates each value of the predicted PRDs obtained by our scheme versus Sabah's in condition of "extrapolated" and "interpolated" CRs. From column comparison, we justify that the GM(1, 1) prediction model performs well for the "extrapolated" CRs and presents closer predicted results in contrast with those of real PRD values in **Table 3**; most notably, if CRs become large enough, higher order polynomial fittings can be less reliable than predicting the "interpolated" time points while the functional fittings make less sense for extrapolated points, that is an auxiliary reason for using the gray system model on prediction.

	CR	4.0	8.0	12.0	16.0	20.0
PRD	Sabah	3.85	7.31	10.7	14.1	17.5
	Proposed	2.96	5.87	8.24	11.5	14.2
	CR	21.0	23.0	25.0	27.0	29.0
PRD	Sabah	18.3	20.0	21.6	23.3	24.9
	Proposed	14.9	16.3	17.6	18.9	20.2

Table 4. Predicted PRD (by GM(1,1)) of the proposed scheme versus Sabah's.

The third set of experiments illustrates the simulations of extracting FECG from MECG with additive noise with an adaptive least mean square (LMS) noise canceller to perform this task, which are depicted in **Figure 6** as modified from Dr. Igal A. Sebag's example [39] on both maternal and fetal heartbeat detections using sample synthetic ECG data. The six subplots permuted in the top row and in the middle row of **Figure 6** show the measuring procedure till the recovery of fetal heartbeat, where the convergence of adaptive noise cancellation takes up to 5–6 s on average. With the assumptions on a sampling rate of 4000 Hz and time duration of 40 s, the maternal heart rate is 89 beats per minute (bpm), and the fmSNR is adjusted as approximately −11.5 dB so as to simulate a test example on the third trimester of pregnancy. The fetal heart rate (FHR) is apparently faster than that of the mother's, normally ranging from 120 to 160 bpm and descending with the progress of gestational weeks. Since the measured FECG via abdominal recordings is often dominated by the maternal heartbeat signal propagating from the chest cavity to maternal abdomen, such path of propagation is constructed as a finite impulse response (FIR) filter with 10 randomized coefficients, with uncorrelated additive random noise which is 0.02 time of the original signal. While the reference signal of MECG is still surrounded with noise, an adaptive LMS filter with 15 coefficients and a step size of 0.00007 can be applied for simplicity of use. Note that the remainder of the error signal after the convergence of the system indicates an estimate of the fetal heartbeat signal associated with the measurement noise.

The bottom row of **Figure 6** comprises three subplots, where the left one shows the filtered FECG in contrast to its reference, the middle one indicates peak detection by applying dynamic thresholds to the filtered FECG and using vertical lines to mark each peak on any FECG signal

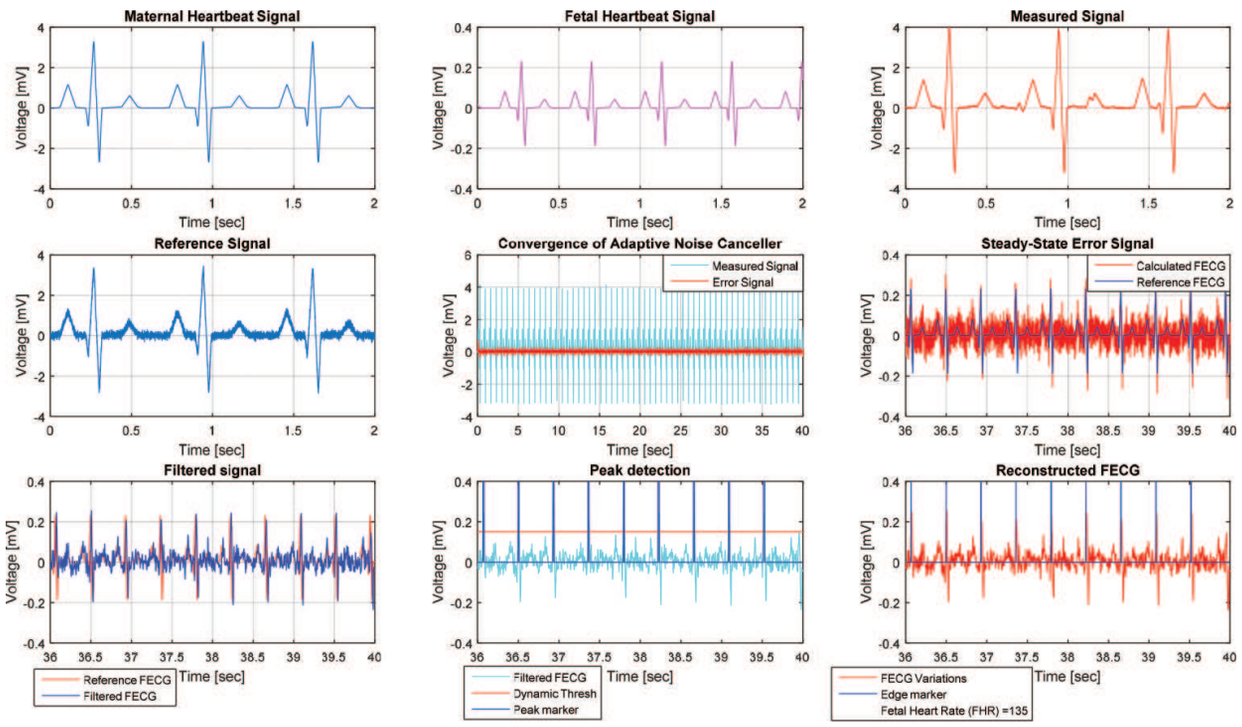

Figure 6. Automatic fetal heart rate detection on the reconstructed FECG from the original heartbeat signals of both mother and fetus.

crossing the threshold, and the right one depicts the reconstructed FECG data with variations and the automatically calculated FHR equals 135 bpm during the time interval of 36–40 s, which coincides with those normal diagnostic examples in FHR monitoring before delivery.

The experiments were conducted and retested via the software platform of MATLAB R2011a and higher versions in a Dell laptop with Core i7-4500U 1.80G CPU and 8GB RAM. We plan to include some specific analysis on the single-channel recordings for both healthy and pathological patients during the second and third trimester of pregnancy, and how the theoretical noninvasive FECG extraction algorithms influence the reconstruction accuracy of ECG signals from clinical experiments in later investigations.

Simulations on a real-life monitoring case were included in the two diagrams of **Figure 7**, where the occurrence of a typical scene on fetal hypoxia was illustrated in types of two parameters such as FHR (ranging from 70 to 150 bpm) and T/QRS (30 samples) in a 10-min

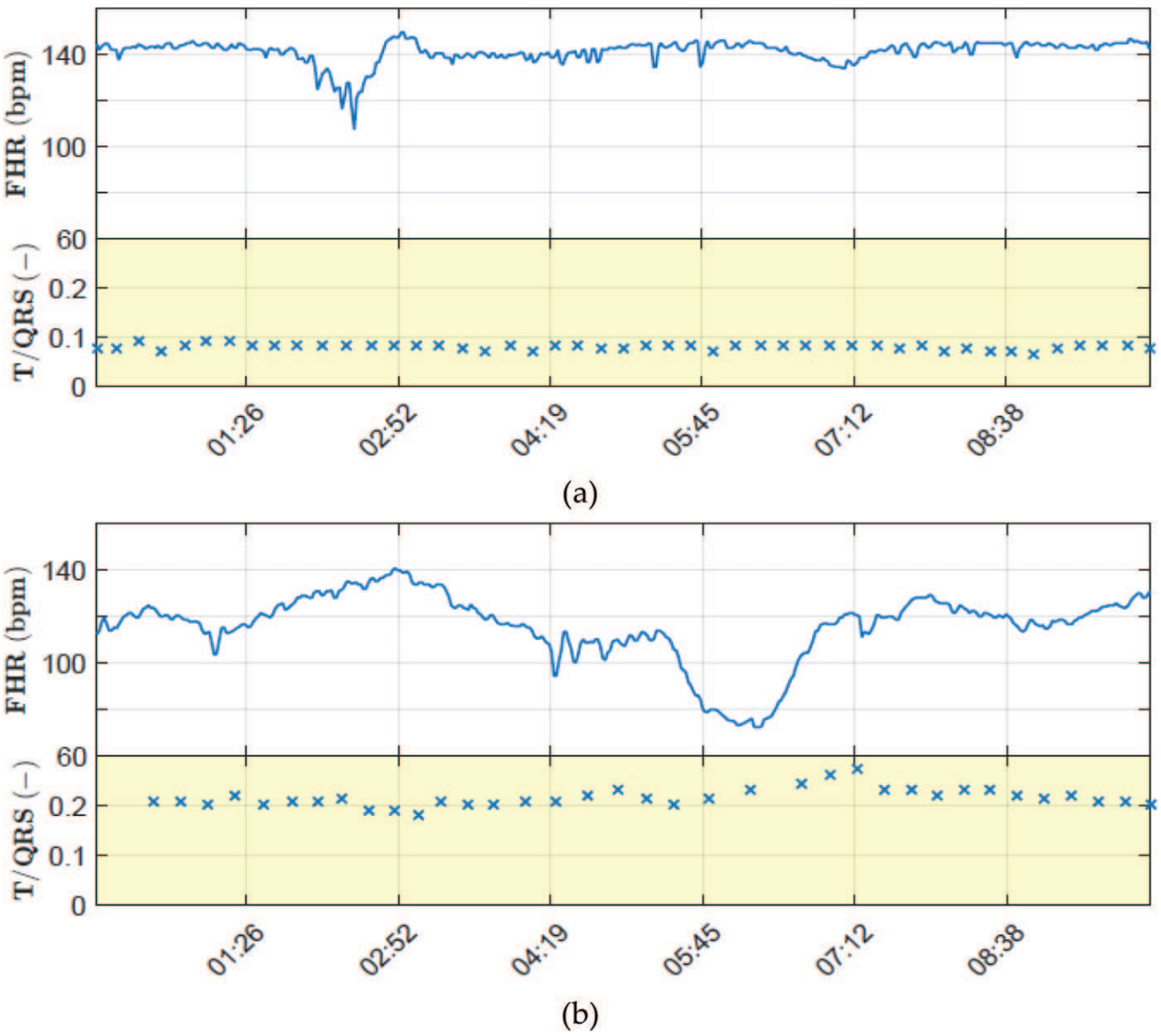

Figure 7. Simulations of sample data on FHR and T/QRS [43] in a 10-min time sequence for cases of: (a) physiological recordings (top); and (b) pathological recordings (bottom).

recording [43]. The top diagram and the bottom diagram depict recordings of a physiological sample and a pathological sample, respectively. Relatively steady FHR in **Figure 7(a)** indicates fetus in good condition, while the large valley in the waveform of FHR (especially at around the time of minute 06:00) in **Figure 7(b)** exhibits the abnormal oscillations of fetal heartbeats resulting from intrauterine hypoxia. For the physiological sample, the parameters are comparatively stable in which FHR displays fluctuations around 140 bpm at most of the time and T/QRS indicates minor numerical vibrations around 0.1; for the pathological sample, FHR exhibits larger amplitude of oscillations ranging from 70 to 140 bpm, while the numerical value of balance point on T/QRS fluctuations is around 0.2. In this trial, it is concluded that the value of fmSNR represents the most crucial factor affecting the quality of filtration, while both the parameter settings on the adaptive filtering system and the locations of electrodes contribute to the signal outputs on abdominal recordings [43].

5. Conclusions

A concise study of recent noninvasive FECG detection schemes has been established in this chapter. We have investigated a variety of algorithms for both single-channel and multichannel noninvasive FECG separation from MECG in abdominal recordings. The extended Kalman-based approach with algorithm variations modeled nonlinearity in single-channel cases, achieved considerably good performance on both synthetic and real-life ECG data. The extended Kalman smoother with ANFIS displays the best overall results on the set of performance metrics among nine noninvasive methods for FECG detection.

We have proposed a scheme of twin-*R* correlative prediction by applying (4, 2) LWT that effectively exploits correlation characteristics of time-domain ECG for sequential data processing. We have feasibly realized the parameter evaluation of ECG compression by building up a predictive GM(1, 1) model in order to give solutions to PRDs with both extrapolated and interpolated CRs, and achieved lower distortion rates in contrast to those of Sabah's. The correlation predictor with the multivariable gray model displays validity and efficiency for compression, suggesting a prospective technique for ECG data prediction and parameter evaluation. The modified simulation trials on fetal heartbeat detection by reconstructing FECG from maternal abdominal recordings via adaptive noise cancellation, provide an example on automatic FHR estimation on synthetic ECG data [39]; sample trials for either physiological case or pathological case on FHR recordings with modeling of hypoxia on mature fetus were included and reported in adaptive control systems for noninvasive monitoring [43].

As future work, we plan to improve one of the recent noninvasive FECG detection schemes by collaborating high-order dimensional data mining (i.e., inducing robust tensor decompositions to the dynamic filter-based models) to the ICA-based JADE scheme for FECG extraction from multichannel abdominal recordings, and updating the prediction system via statistical machine learning other than ANFIS, where the cocktail party-based solutions suggest a feasible tool for technical improvements [40]. We also plan to design an analytical software platform using the wavelet toolbox, which is oriented for detecting fetal cardiac arrhythmias with more practical trials on real data toward the multilead system for abdominal ECG recordings.

Author details

Xin Gao

Address all correspondence to: xgao1985@email.arizona.edu

Department of Electrical and Computer Engineering, the University of Arizona, Tucson, USA

References

[1] Adithya PC, Sankar R, Moreno WA, Hart S. Trends in fetal monitoring through phonocardiography: Challenges and future directions. Biomedical Signal Processing and Control. 2017;**33**:289–305

[2] Andreotti F, Riedl M, Himmelsbach T, Wedekind D, Wessel N, Stepan H, Schmieder C, Jank A, Malberg H, Zaunseder S. Robust fetal ECG extraction and detection from abdominal leads. Physiological Measurement. 2014;**35**(8):1551–1568

[3] Assaleh K. Extraction of fetal electrocardiogram using adaptive neuro-fuzzy interference systems. IEEE Transactions on Biomedical Engineering. 2007;**54**(1):59–68

[4] Behar J, Johnson A, Clifford GD, Oster J. A comparison of single channel fetal ECG extraction methods. Annals of Biomedical Engineering. 2014;**42**(6):1340–1353

[5] Behar J, Oster J, Clifford GD. Non-invasive FECG extraction from a set of abdominal sensors. In: IEEE Conference of Computing in Cardiology (CinC); September 22–24; Zaragoza, Spain. IEEE; 2013. pp. 197–200

[6] Clifford GD, Sameni R, Ward J, Robinson J, Wolfberg AJ. Clinically accurate fetal ECG parameters acquired from maternal abdominal sensors. American Journal of Obstetrics and Gynecology. 2011;**205**(1):47.e1–47.e5

[7] Clifford GD, Silva I, Behar J, Moody GB. Non-invasive fetal ECG analysis. Physiological Measurement. 2014;**35**(8):1521–1536

[8] Gao X. On the improved correlative prediction scheme for aliased electrocardiogram (ECG) data compression. In: 2012 Annual International Conference of the IEEE Engineering in Medicine and Biology Society (EMBC); August 28-September 01; San Diego, CA, USA. 2012. pp. 6180–6183

[9] Ghodsi M, Hassani H, Sanei S. Extracting fetal heart signal from noisy maternal ECG by singular spectrum analysis. Journal of Statistics and its Interface, Special Issue on the Application of SSA. 2010;**3**(3):399–411

[10] Hyvarinen A. Fast and robust fixed-point algorithms for independent component analysis. IEEE Transactions on Neural Networks. 1999;**10**(3):626–634

[11] Immanuel JJR, Prabhu V, Christopheraj VJ, Sugumar D, Vanathi PT. Separation of maternal and fetal ECG signals from the mixed source signal using FASTICA. Procedia Engineering. 2012;**30**:356–363

[12] Jafari MG, Chambers JA. Fetal electrocardiogram extraction by sequential source separation in the wavelet domain. IEEE Transactions on Biomedical Engineering. 2005;**52** (3):390–400

[13] Jalaleddine SMS, Hutehens CG, Strattan RD, Coberly WA. ECG data compression techniques−−A unified approach. IEEE Transactions on Biomedical Engineering. 1990;**37** (4):329–343

[14] Kropfl M, Modre-Osprian R, Schreier G, Hayn D. A robust algorithm for fetal QRS detection using non-invasive maternal abdominal ECGs. Computing in Cardiology. 2013;**40**:313–316

[15] Kumar P, Sharma SK, Prasad S. Detection of FECG from multivariate abdominal recordings using wavelets and neuro-fuzzy systems. International Journal of Engineering and Advanced Technology Studies. 2013;**2**(1):45–51

[16] Lathauwer L, Moor B, Vanderwalle J. Fetal electrocardiogram extraction by blind source subspace separation. IEEE Transactions on Biomedical Engineering. 2000;**47**(5):567–572

[17] Guerrero-Martinez JF, Martinez-Sober M, Bataller-Mompean M, Magdalena-Benedito JR. New algorithm for fetal QRS detection in surface abdominal records. Computers in Cardiology. 2006;**33**:441–444

[18] Melillo P, Santoro D, Vadursi M. Detection and compensation of inter-channel time offsets in indirect fetal ECG sensing. IEEE Sensors Journal. 2014;**14**(7):2327–2334

[19] Panigrahy D, Sahu PK. Extraction of fetal electrocardiogram (ECG) by extended state Kalman filtering and adaptive neuro-fuzzy inference system (ANFIS) based on single channel abdominal recording. Sadhana. 2015;**40**(Part 4):1091–1104

[20] Peters CHL, Van Laar JOEH, Vullings R, Oei SG, Wijn PFF. Beat-to-beat heart rate detection in multi-lead abdominal fetal ECG recordings. Medical Engineering & Physics. 2012;**34**(3):333–338

[21] Poian GD, Bernardini R, Rinaldo R. Separation and analysis of fetal-ECG signals from compressed sensed abdominal ECG recordings. IEEE Transactions on Biomedical Engineering. 2016;**63**(6):1269–1279

[22] Reza S, Shamsollahi MB, Jutten C, Clifford GD. A nonlinear Bayesian filtering framework for ECG denoising. IEEE Transactions on Biomedical Engineering. 2007;**54**(12):2172–2185

[23] Rooijakkers MJ, Rabotti C, de Lau H, Oei SG, Bergmans JWM, Mischi M. Feasibility study of a new method for low-complexity fetal movement detection from abdominal ECG recordings. IEEE Journal of Biomedical and Health Informatics. 2016;**20**(5):1361–1368

[24] Rosén KG, Amer-Wåhlin I, Luzietti R, Norén H. Fetal ECG waveform analysis. Best Practice & Research Clinical Obstetrics & Gynaecology. 2004;**18**(3):485–514

[25] Rosén KG, Samuelsson A. Device for reducing signal noise in a fetal ECG signal. U.S. Patent 6658284, issued December 2, 2003

[26] Santiago MC. Processing of Abdominal Recordings by Kalman Filters [Internet]. 2012. Available from: https://upcommons.upc.edu/bitstream/handle/2099.1/16148/Final_Project_Marcos_Cruz_Processing_of_abdominal_recordings_by_Kalman_filters.pdf

[27] Selvaraj R, Kanagaraj B. A multi-stage adaptive singular value decomposition approach for fetal ECG signal extraction in multichannel input system for prenatal health monitoring. Asian Journal of Information Technology. 2016;**15**(6):1049–1055

[28] Silva I, Behar J, Sameni R, Zhu T-T, Oster J, Clifford GD, Moody GB. Noninvasive fetal ECG: The PhysioNet/computing in cardiology challenge 2013. In: IEEE Conference of Computing in Cardiology (CinC); September 22–24. 2013. pp. 149–152

[29] Song S, Rooijakkers MJ, Harpe P, Rabotti C, Mischi M, van Roermund AHM, Cantatore E. A noise reconfigurable current-reuse resistive feedback amplifier with signal-dependent power consumption for fetal ECG monitoring. IEEE Sensors Journal. 2016;**16**(23):8304–8313

[30] Tadi MJ, Lehtonen E, Hurnanen T, Koskinen J, Eriksson J, Pänkäälä M, Teräs M, Koivisto T. A real-time approach for heart rate monitoring using a Hilbert transform in seismocardiograms. Physiological Measurement. 2016;**37**(11):1885–1909

[31] Taylor MJO, Smith MJ, Thomas M, Green AR, Cheng F, Oseku-Afful S, Wee L-Y, Fisk NM, Gardiner HM. Non-invasive fetal electrocardiography in singleton and multiple pregnancies. BJOG: An International Journal of Obstetrics & Gynaecology. 2003;**110**(7):668–678

[32] Yeh H-M, Chang Y-C, Lin C, Yeh C-H, Lee C-N, Shyu M-K, Hung M-H, et al. A new method to derive fetal heart rate from maternal abdominal electrocardiogram monitoring fetal heart rate during cesarean section. PLoS One. 2015;**10**(2):e0117509

[33] Yu S-H. Detection of fetal cardiac repolarization abnormalities using magneto-cardiography [Ph.D. Dissertation]. The University of Wisconsin-Madison; 2013

[34] Zarzoso V, Nandi AK. Noninvasive fetal electrocardiogram extraction blind separation versus adaptive noise cancellation. IEEE Transactions on Biomedical Engineering. 2001;**48**(1):12–20

[35] Zheng W, Li X-L, Wei X-Y, Liu H-X. Foetal ECG extraction by support vector regression. Electronic Letters. 2016;**52**(7):506–507

[36] Zheng W, Wei X-Y, Zhong J-J, Liu H-X. Fetal heart beat detection by Hilbert transform and non-linear state-space projections. IET Science, Measurement & Technology. 2015;**9**(1):85–92

[37] Zhong Y-D. Blind adaptive filtering for extraction of fetal ECG from maternal abdominal ECG [Ph.D. Dissertation]. The University of Illinois at Chicago; 2007

[38] https://en.wikipedia.org/wiki/Data_compression_ratio

[39] https://www.mathworks.com/matlabcentral/fileexchange/35328-simulink-model-for-fetal-ecg-extraction--hdl-compatible-algorithm-/content/mom_and_fetus.m

[40] https://cran.r-project.org/web/packages/JADE/vignettes/JADE-BSSasymp.pdf

[41] https://www.cablesandsensors.com/pages/12-lead-ecg-placement-guide-with-llustrations

[42] Lynn WD, Escalona OJ, McEneaney DJ. Arm and wrist surface potential mapping for wearable ECG rhythm recording devices: A pilot clinical study. Sensors & their Applications, Journal of Physics: Conference Series. 2013;**450**:012026. DOI: 10.1088/1742-6596/450/1/012026; http://iopscience.iop.org/article/10.1088/1742-6596/450/1/012026/pdf

[43] Martinek R, Kahankova R, Nazeran H, Konecny J, Jezewski J, Janku P, Bilik P, Zidek J, Nedoma J, Fajkus M. Non-invasive fetal monitoring: A maternal surface ECG electrode placement-based novel approach for optimization of adaptive filter control parameters using the LMS and RLS algorithms. Sensors. 2017;**17**(5):1154. http://www.mdpi.com/1424-8220/17/5/1154